Journal of Materials Chemistry A

Accepted Manuscript

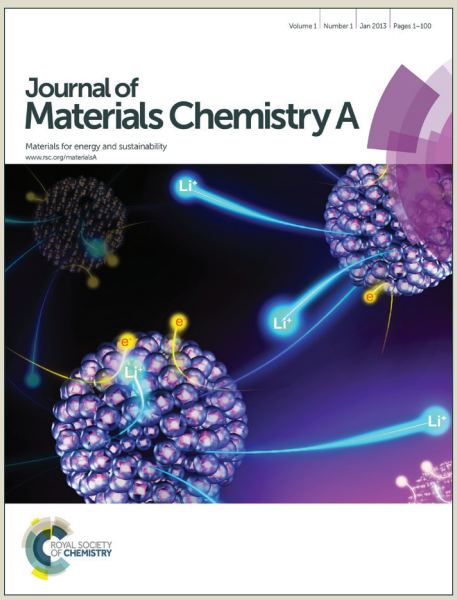

ROYAL SOCIETY OF CHEMISTRY

www.rsc.org/materialsA

Graphical Abstract

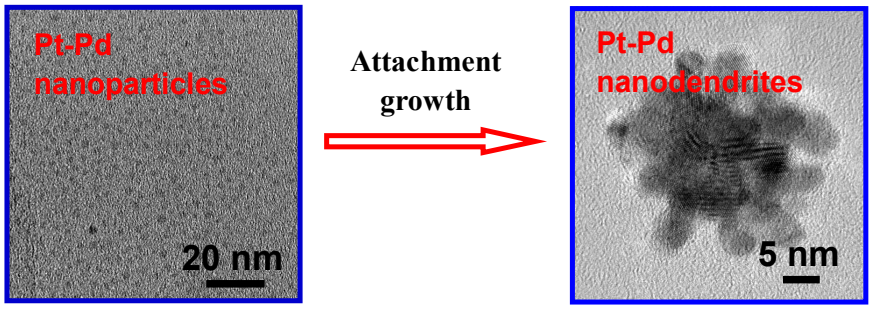

Porous Pt-Pd nanodendrites were fabricated by a co-chemical reduction method using both PVP and urea as the co-stabilizing and co-structure-directing agents. The Pt-Pd nanodendrites displayed high catalytic activity and stability toward the electrooxidation of methanol and ethylene glycol in alkaline media.

Facile synthesis of Pt-Pd nanodendrites and their superior electrocatalytic activity

Jing-Jing Lv, Jie-Ning Zheng, Shan-Shan Li, Li-Li Chen, Ai-Jun Wang*, Jiu-Ju Feng*

College of Geography and Environmental Science, College of Chemistry and Life Science, Zhejiang Normal University, Jinhua 321004, China

*Corresponding Author: jjfeng@zjnu.cn (JJF), ajwang@zjnu.cn (AJW); Tel./Fax: +86 579 82282269.

Abstract:

In this report, well-dispersed porous Pt-Pd nanodendrites (Pt-Pd NDs) were synthesized at high yield by a simple one-pot wet chemical method without using any seed, template, or toxic organic solvent. Poly(vinylpyrrolidone) (PVP) and urea were employed as the co-stabilizing and co-structure-directing agents. It was found that the reaction temperature, the amount of PVP and urea, the Pt/Pd molar ratio, and the pH value of the reaction media greatly affected the size and shape of the Pt-Pd product. The as-prepared Pt-Pd nanocrystals had the larger active surface area, superior catalytic activity, and better stability for the electrooxidation of methanol and ethylene glycol (EG), compared with the commercial Pt-black and Pd-black catalysts.

Keywords: Pt-Pd nanodentrites, electrocatalytic activity, methanol, ethylene glycol

Introduction

To date, Pt and Pt-based nanostructures have attracted increasing research attention because of their wide applications in chemical reactions, sensors and fuel cells.[1-5] However, there is still a long way to realize their practical applications for the sky-rocketing price and the scarcity of Pt. To overcome these barriers, it is necessary to alloy a second metal (M = Pd, Fe, Ni, Co, etc.) to maximize the activity.[2, 6-8]

The last decades have witnessed the preparation of many Pt-Pd alloy nanocrystals with different shapes such as cages,[9] wires,[10] icosahedra,[11] tetrahedral,[12] dendrites,[13] clusters,[14] octahedral[15] and cubes.[16] Accordingly, many methods have been developed such as co-chemical reduction,[3] seed mediated growth,[17] electrochemical deposition[18] and galvanic replacement.[19] For example, Lim et al. synthesized Pt-Pd nanodendrites using Pd nanoparticles as seeds.[17] Zhang and his coworkers prepared Pt-Pd alloys with selective shapes by a one-pot solvothermal method.[16] Nevertheless, the above methods suffer from relatively high cost, complex reaction steps, and rigorous operation skills. Fortunately, wet-chemical synthesis is thought to be the best route for precise control of the Pt-Pd alloy nanostructures and relatively nontoxic to the environment.[20] Therefore, it's always desirable to explore more economic, facile, and environmentally friendly solution-phase approaches in the synthesis of Pt-Pd nanostructures with superior properties.

Compared with the previous reports,[1, 5, 21] we developed a facile and environmentally friendly one-pot wet chemical method to synthesize porous Pt-Pd nanodentrites (Pt-Pd NDs) by using poly(vinylpyrrolidone) (PVP) and urea as the

co-stabilizing and co-structure-directing agents. No toxic organic solvent, seed, or template is involved. The electrocatalytic activity and stability of the Pt-Pd NDs were investigated in some detail, using the oxidation of methanol and ethylene glycol (EG) as model systems.

Experimental section

Chemicals

Chloroplatinic acid ($H_2PtCl_6·6H_2O$), palladium chloride ($PdCl_2$), PVP (MW = 58 000), urea, hydrazine hydrate (16.5 M), commercial Pt black and Pd black catalysts were purchased from Shanghai Aladdin Chemical Reagent Company (Shanghai, China). All the other chemicals were analytical grade and used without further purification. All aqueous solutions were prepared with twice-distilled water.

Synthesis of the porous Pt-Pd nanodendrites

For the typical synthesis of the Pt-Pd NDs, 0.50 mL of 100 mM $PdCl_2$, 1.29 mL of 38.62 mM $H_2PtCl_6·6H_2O$, and 0.015 g urea were put into a 10 mL of 0.25 wt % PVP solution under stirring. Afterwards, the pH of the mixed solution was adjusted to 12 by freshly prepared 0.1 M NaOH. Then, the mixture was placed into the ice-bath and turned black quickly after the addition of 100 uL hydrazine hydrate (16.5 M) under stirring. The black solution was further stirred for another 1 h under the ice-bath. Finally, the black precipitate was collected by centrifugation, thoroughly washed with ethanol and water to remove the residual PVP, and dried at 60 °C in a vacuum.

Characterization

The morphology, composition, and elemental distribution of the deposits were characterized by transmission electron microscopy (TEM), high-resolution TEM (HRTEM) images, X−ray energy dispersive spectrum (EDS) and high angle annular dark field-scanning transmission electron microscopy (HAADF-STEM) on a JEM−2010HR transmission electron microscope coupled with an energy-dispersive X−ray spectrometer (Dxford−1NCA). TEM analysis was carried out at an accelerating voltage of 200 kV, and Cu grids were used as substrates. A small amount of the black sample was dispersed in ethanol by ultrasonication, and then a drop of the suspension was deposited onto a Cu grid for TEM observation. The crystal structures were examined by X-ray diffraction (XRD) analysis on a Bruker-D8-AXS diffractometer system equipped with Cu Kα radiation (Bruker Co., Germany) and X-ray photoelectron spectroscopy (XPS) measurements performed by a thermofisher-ESCALab 250 (ThermoFisher, E. Grinstead, UK), using Al Kα X-ray radiation (1486.6 eV) for excitation.

Electrochemical measurements

All electrochemical experiments were performed on a CHI 660D electrochemical workstation (CH Instruments, Chenhua Co., Shanghai, China), and performed on a conventional three-electrode cell, which includes a platinum wire as counter electrode, a saturated calomel electrode (SCE) as reference electrode, and a bare or modified glassy carbon electrode (GCE) as working electrode.

For preparation of the Pt-Pd NDs modified electrode, 3.0 mg of the Pt-Pd NDs were added into 1 mL water under ultrasonication for 30 min to obtain a uniform suspension. Then, 10 uL of the suspension was placed onto the electrode surface by a macrosyringe and dried in air. Next, the electrode was coated with 10 uL of 0.05 % Nafion solution. For comparison, the commercial Pt-black and Pd-black catalysts modified electrodes were prepared with the similar procedures. Thus, the specific loading of the catalysts was 0.424 mg cm^{-2} on the electrode surface.

Electrochemical CO-stripping voltammograms were obtained by oxidizing pre-adsorbed CO (CO_{ad}) in 0.5 M H_2SO_4 at a scan rate of 50 mV s^{-1}. Here, the specific loading of the catalysts was 0.509 mg cm^{-2}. The CO was purged through the 0.5 M H_2SO_4 solution for 30 min to allow complete adsorption of CO onto the deposit. The amount of the adsorbed CO was evaluated by integrating the CO_{ad} stripping peak and correcting for the capacitance of the double electric layer. The cyclic voltammetric experiments for methanol and EG oxidation were carried out in 1.0 M KOH at a scan rate of 50 mV s^{-1}. The chronoamperometric experiments were conducted at a given potential of –0.2 V in 1.0 M KOH + 1.0 M methanol and 1.0 M KOH + 1.0 M EG. All experiments were conducted at room temperature, if not stated otherwise.

Results and discussion

Physical characterization

Fig. 1A shows a variety of well-defined Pt-Pd NDs with an average diameter of 19.5

nm, which have a very narrow size distribution from 13 to 26 nm (inset in Fig. 1A). Furthermore, each dendrite has porous nanostructures, containing several subunits (Fig. 1B). And its polycrystalline nature is manifested by the selected-area electron diffraction pattern (inset in Fig. 1B). Besides, HRTEM images illustrate the lattice spacing distances of ca. 0.224 nm, 0.225 nm and 0.195 nm from the blue square areas marked in the Pt-Pd nanodendrite (Fig. 1C-F), which are close to the (111) and (200) planes of face-centered cubic (fcc) Pt-Pd alloy, respectively.[16, 22] Furthermore, the lattice spacing distances were between single Pt (0.2650 nm, 0.1962 nm) and Pd (0.2246 nm, 0.1945 nm) standard patterns, confirming the formation of the solid-solution nanostructures of the PtPd NDs.

As shown in Fig. 2, the HAADF-STEM-EDS mapping image and line scanning profiles were recorded to examine the elemental distribution of the Pt-Pd nanodendrite. It is evident that Pt and Pd are homogeneously distributed across the whole nanodendrite (Fig. 2A-C). Moreover, the compositional line scanning profiles further demonstrate their homogeneous distribution (Fig. 2D), which also show the formation of the solid-solution Pt-Pd alloy.[21]

XRD (Fig. 3A) and EDS (Fig. 3B) measurements were performed to investigate the composition and crystal structures of the Pt-Pd NDs. The EDS confirmed the presence of Pt and Pd atoms. In the XRD spectra, the representative diffraction peaks at 39.9°, 46.4°, 68.0°, and 81.7° are well assigned to the (111), (200), (220), and (311) planes of the fcc Pt-Pd alloy,[23] respectively. These peaks are coincidently located between single Pt (JCPDS-04-0802 Pt) and Pd (JCPDS-46-1043 Pd),[24] indicating the

formation of the solid-solution Pt-Pd alloy, as supported by the HRTEM results (Fig. 1D-F). This observation is similar to the PtPd nanocubes and PtPd nanowires fabricated previously.[7, 10]

Fig. 3C and D show the XPS spectra of Pt 4f and Pd 3d for the Pt-Pd NDs, which can be divided into two pairs of Lorentzian curves. The peaks from 71.44 eV (Pt $4f_{7/2}$), 74.67 eV (Pt $4f_{5/2}$), 72.89 eV (Pt $4f_{7/2}$), and 77.26 eV (Pt $4f_{5/2}$) are attributed to Pt^0 and Pt^{II} species, respectively, while the peaks from 355.76 eV (Pd $3d_{5/2}$), 340.99 eV (Pd $3d_{3/2}$), 337.87 eV (Pd $3d_{5/2}$), and 343.48 eV (Pd $3d_{3/2}$) are assigned to Pd^0 and Pd^{II} species.[25] These values are in good agreement with those of the Pt-Pd porous nanorods.[26] Furthermore, in terms of their peak intensity, it can be concluded that Pt^0 and Pd^0 are the predominant species, revealing complete reduction of $PtCl_6^{2-}$ and Pd^{2+} in the present synthesis.

To have a deep insight on the formation mechanism of the Pt-Pd NDs, a series of control experiments were investigated in some detail. Firstly, the reaction temperature plays the key role in the kinetic control of nucleation and growth in our case. Specifically, the quality and yield of the Pt-Pd products decrease with the increase of the reaction temperature within 60 °C (Fig. S1A-C), which are different from that prepared at the standard temperature of 0 °C (Fig. 1A), while other conditions are unchanged. Further increasing the temperature to 80 °C fails to produce any Pt-Pd dendrite (Fig. S1D). This is ascribed to significant deviation from the quasi-thermodynamic equilibrium state induced by the increase of the temperature. Moreover, increasing the reaction temperature causes the decrease of the viscosity in

the solution and the increase of the molecular disordered movement along with diffusion rate, leading to serious desorption of the adsorbed PVP and urea from the surface of the Pt-Pd nanocrystals, indicating that low temperature is beneficial to the well micellar structures of PVP.[27] When the reaction temperature is up to 80 °C, the micellar structures become disordered in some degree. As a result, the as-formed NPs have poor dispersion by increasing the temperature (Fig. S1 and Fig. 1A). Thus, low temperature facilitates the formation of the productive and well-defined Pt-Pd nanostructures, similar to the previous report.[28]

More importantly, the absence of PVP yields heavily aggregated Pt-Pt particles, while other conditions were kept the same (Fig. S2A). Furthermore, using much less or more PVP would produce the Pt-Pd NDs with poor quality (Fig. S2B, C). It indicates the key role of PVP as a capping agent. The presence of PVP can protect the nanocrystals from aggregation and even enhance the shape-controlled synthesis, leading to the formation of well-defined Pt-Pd NDs with good dispersity.[29, 30] Similarly, the absence of urea only yields some approximately spherical nanoparticles, while nearly no dendritic-like nanostructures emerged (Fig. S3A). With the increase of the urea concentration, the quality of the Pt-Pd NDs is gradually improved, whereas the porosity degree drops down (Fig. S3B-D). It is noticed that individual PVP or urea hardly produces the Pt-Pd NDs. Therefore, the coexistence of PVP and urea synergistically play the critical roles in the present work, owing to selective binding of PVP and urea on the specific crystal surface during the growth process.[31]

The pH value of the reaction media was also manifested great effects on the

morphology of the Pt-Pd products. Similar Pt-Pd NDs are also formed in acid media, similar to those in alkaline media, whereas their porosity degree is decreased (Fig. S4A). Impressively, irregular spherical Pt-Pd nanoparticles with toothed edges are generated in neutral solution (Fig. S4B). These phenomena are due to the protonation and deprotonation of the adsorbed molecules on the Pt-Pd nanoparticles in acid and basic media, respectively. Moreover, the protonation and deprotonation are strongly correlated with the pH values, leading to the formation of different nanostructures at different pH values.[32]

It's known that bimetallic nanocrystals have preferable property over single metal, because the tunable chemical compositions in a wide range would bring synergistic effects in catalytic applications.[33] To our knowledge, the standard reduction potential of the Pd^{2+}/Pd pair is 0.92 V, which is higher than that of the $PtCl_6^{2-}$/Pt (0.73 V). Thus, it is possible that Pd nuclei may form at the very initial stage, and the newly generated Pd atoms would induce the co-reduction of $PtCl_6^{2-}$ to form Pt-Pd alloyed nanocrystals.

To confirm this assumption, using individual $PdCl_2$ (Fig. 4A) as precursors, while other conditions were kept constant, the product contains some irregular dendrites with multiple sub-branches, indicating that the Pd nuclei motivate the formation of the Pt-Pd NDs. Alternatively, using H_2PtCl_6 as a precursor (Fig. 4B), the sample is only composed of several large heavy aggregates. Furthermore, the Pt-Pd alloy nanostructures were synthesized with different molar ratios of Pt to Pd (Pt/Pd). When the Pt/Pd molar ratio is increased to 2:1 (Fig. 4C), some irregular and solid

particles are produced, while no any dendrite formed, because of the weak inducement capacity from less Pd content. On the other hand, the Pt-Pd NDs own lower porosity degree as the Pt/Pd molar ratio is 1:2 (Fig. 4D), which may be result from the attenuation of synergistic effects between Pt and Pd.[31]

Fig. 5 illustrates the formation mechanism of the Pt-Pd NDs based on the rapid nucleation and particle attachment growth.[3, 34] At the very initial stage, abundant Pt and Pd atoms are immediately produced upon the addition of hydrazine hydrate. As soon as the atomic Pt and Pd concentrations have reached hyper-saturated states, dense nuclei are formed through the self-aggregation process to minimize the total surface free energy of the system. Next, with the co-directing effects of PVP and urea, the nuclei were self-organized by twinning and imperfect oriented attachment to form the dendritic nanostructures. As time elapsing, the growth rate is dropped down and the newly formed Pt-Pd hybrid crystals deposit onto the initial ones, and finally blossom into mature nanodendrites (Fig. 1A-C).[6, 20, 35, 36]

The time-dependent morphology evolution was strongly supported by TEM measurements. As shown in Fig. 6, vast dense nuclei are emerged after the addition of the reductant only for 1 min (Fig. 6A). The nuclei are soon growing into nanodendrites with the assistance of PVP and urea as the co-directing agents in another 4 min (Fig. 6B). Then, the newly produced Pt-Pd tiny particles are gradually attached to the branches (within 30 min) and grown into well-defined Pt-Pd NDs (Fig. 6C). Full-growth and stable Pt-Pd NDs are formed by extending the time to 1 h or even 2 h (Fig. 6D).

Electrocatalytic measurements

The CO-stripping measurements were performed to estimate the electrochemically active surface area (EASA) of the Pt-Pd NDs modified electrodes (Fig. 7A), with the Pt-black (Fig. 7B) and Pd-black (Fig. 7C) catalysts modified electrodes as the references. The EASA of the Pt-Pd NDs is estimated to be 92.0 m^2 g^{-1}, which is markedly larger than those of the Pt black (7.0 m^2 g^{-1}) and Pd black (11.6 m^2 g^{-1}) catalysts, owing to the porous structures providing additional internal surfaces for small molecules available. Large EASA always enhances the catalytic performance, which is very important to the electrochemical activity of the Pt-Pd NDs.[37] Meanwhile, the cyclic voltammgrams (CVs) are recorded on the Pt-Pd NDs (curve a), Pt black (curve b), and Pd black (curve c) catalysts modified electrodes in 0.5 M H_2SO_4 (Fig. S5), which show that the increased current densities in the hydrogen adsorption/desorption and oxide formation/reduction regions in the order of the Pt-Pd NDs, Pt black, and Pd black catalysts, indicating larger EASA of the Pt-Pd NDs.[24]

It is known that Pt or Pd-based nanocrystals have superior electrocatalytic activity toward ethanol or methanol oxidation in alkaline media.[5, 10, 15, 38-42] The electrocatalytic performance of the Pt-Pd NDs modified electrode was examined by cyclic voltammetry in 1.0 M KOH containing 1.0 M methanol (Fig. 8A) and 1.0 M EG (Fig. 8B). For methanol oxidation, there is an oxidation peak observed in the forward scan, corresponding to the oxidation of freshly chemisorbed methanol. And another anodic peak is detected in the reverse sweep, which are attributed to the removal of carbonaceous species that are not completely oxidized in the forward

scan.[43] For comparison, the CVs of the Pt-black and Pd-black catalysts modified electrodes were also recorded under the identical conditions. The catalytic current density of the Pt-Pd NDs is 3.05, 16.3, and 1.85 times higher than that on the Pt-black and Pd-black catalysts, and the Pt-Pd alloy nanosponges in the literature,[44] respectively. Furthermore, the ratio of the forward peak current density (j_F) to the reverse one (j_R) is up to 3.5, similar to the Pd black (3.2) and Pt black (4.5) catalysts. However, this value is much higher than that on the PdPt@Pt/C (1.04) in previous work,[45] which can be ascribed to good CO tolerance of the Pt-Pd NDs.[46] Similar trend is found in the case of EG oxidation. In addition, the onset potential of the Pt-Pd NDs is close to the Pt-black catalyst, but more negative than that on the Pd-black catalyst toward both methanol and EG oxidation, indicating the improved catalytic activity of the Pt-Pd NDs.

The electrochemical stability of the Pt-Pd NDs modified electrodes was investigated by chronoamperometric experiments toward methanol (Fig. 9A) and EG (Fig. 9B) oxidation, along with the Pt-black (curve b) and Pd-black (curve c) catalysts as references. The catalytic current density of the Pt-Pd NDs slowly drops down and still keeps the higher current density even after 4000 s (curve a), while the Pt-black and Pd-black catalysts show a rapid decay and display lower current density under the identical conditions.[47]

The durability of the Pt-Pd NDs modified electrode was confirmed by cyclic voltammetry in 1.0 M KOH containing 1.0 M methanol (Fig. 9C) and 1.0 M EG (Fig. 9D), where the electrocatalytic current density is almost unchanged within 500 cycles.

For methanol oxidation, the Pt-Pd NDs modified electrode remained 72 % and 50 % of its original values after 250 and 500 cycles, respectively. As for EG oxidation, the catalytic current density remained 77 % of its initial value after 500 cycles. These results demonstrate good durability of the Pt-Pd NDs.[48] The strong tolerance, improved electrocatalytic performance, and good stability of the Pt-Pd NDs are attributed to the special structures of the porous Pt-Pd NDs and the synergistic effects between Pt and Pd.[49-51]

Conclusions

In summary, we have developed a simple and facile method for large-scale synthesis of porous Pt-Pd NDs via a one-pot wet chemical strategy, using PVP and urea as the co-stabilizing and co-structure-directing agents. The as-prepared Pt-Pd nanocrystals show enhanced electrocatalytic activity and more reliability toward methanol and EG oxidation, compared with the Pt-black and Pd-black catalysts under the same conditions, which can be attributed to the porous structures of the Pt-Pd NDs and the synergistic effects between Pt and Pd. The as-prepared Pt-Pd NDs might be a new promising electrocatalyst for direct methanol and EG fuel cells. This method can be generalized to produce other noble-metal-based bimetallic nanostructures for catalytic applications.

Acknowledgements

This work was financially supported by the NSFC (21175118 and 21275130) and

Colleges in Zhejiang province to the young academic leaders of academic climbing project (pd2013055).

References

1 A. Chen and P. Holt-Hindle, *Chem. Rev.*, 2010, **110**, 3767.

2 V. Mazumder, M. Chi, K. L. More and S. Sun, *J. Am. Chem. Soc.*, 2010, **132**, 7848.

3 G. Fu, K. Wu, J. Lin, Y. Tang, Y. Chen, Y. Zhou and T. Lu, *J. Phys. Chem. C*, 2013, **117**, 9826.

4 Z. Xu, C. E. Carlton, L. F. Allard, Y. Shao-Horn and K. Hamad-Schifferli, *J. Phys. Chem. Lett.*, 2010, **1**, 2514.

5 N. S. Porter, H. Wu, Z. Quan and J. Fang, *Acc. Chem. Res.*, 2013, **46**, 1867.

6 W. Wang, D. Wang, X. Liu, Q. Peng and Y. Li, *Chem. Commun.*, 2013, **49**, 2903.

7 Y. Lu, Y. Jiang, H. Wu and W. Chen, *J. Phys. Chem. C*, 2013, **117**, 2926.

8 C. Song, Y. Wang and N. L. Rosi, *Angew. Chem.*, 2013, **125**, 4085.

9 H. Zhang, M. Jin, H. Liu, J. Wang, M. J. Kim, D. Yang, Z. Xie, J. Liu and Y. Xia, *ACS Nano*, 2011, **5**, 8212.

10 B. Y. Xia, H. B. Wu, Y. Yan, X. W. Lou and X. Wang, *J. Am. Chem. Soc.*, 2013, **135**, 9480.

11 E. G. Mednikov, M. C. Jewell and L. F. Dahl, *J. Am. Chem. Soc.*, 2007, **129**, 11619.

12 A.-X. Yin, X.-Q. Min, Y.-W. Zhang and C.-H. Yan, *J. Am. Chem. Soc.*, 2011, **133**, 3816.

13 S. Guo, S. Dong and E. Wang, *ACS Nano*, 2009, **4**, 547.

14 S. P. Elangovan, C. Bischof and M. Hartmann, *Catal. Lett.*, 2002, **80**, 35.

15 Y.-W. Lee, A. R. Ko, D.-Y. Kim, S.-B. Han and K.-W. Park, *RSC Advances*, 2012, **2**, 1119.

16 Z.-C. Zhang, J.-F. Hui, Z.-G. Guo, Q.-Y. Yu, B. Xu, X. Zhang, Z.-C. Liu, C.-M. Xu, J.-S. Gao and X. Wang, *Nanoscale*, 2012, **4**, 2633.

17 B. Lim, M. Jiang, P. H. C. Camargo, E. C. Cho, J. Tao, X. Lu, Y. Zhu and Y. Xia, *Science*, 2009, **324**, 1302.

18 I. Choi, S. H. Ahn, J. J. Kim and O. J. Kwon, *Appl. Catal., B*, 2011, **102**, 608.

19 C. Koenigsmann, A. C. Santulli, K. Gong, M. B. Vukmirovic, W.-p. Zhou, E. Sutter, S. S. Wong and R. R. Adzic, *J. Am. Chem. Soc.*, 2011, **133**, 9783.

20 Y. Wang, S.-I. Choi, X. Zhao, S. Xie, H.-C. Peng, M. Chi, C. Z. Huang and Y. Xia, *Adv. Funct. Mater.*, 2013, DOI: 10.1002/adfm.201302339 (ASAP).

21 H. Zhang, M. Jin and Y. Xia, *Chem. Soc. Rev.*, 2012, **41**, 8035.

22 H. Zhang, Y. Yin, Y. Hu, C. Li, P. Wu, S. Wei and C. Cai, *J. Phys. Chem. C*, 2010, **114**, 11861.

23 S. C. Sahu, A. K. Samantara, B. Satpati, S. Bhattacharjee and B. K. Jena, *Nanoscale*, 2013, **5**, 11265.

24 X. Yang, Q. Yang, J. Xu and C.-S. Lee, *J. Mater. Chem.*, 2012, **22**, 8057.

25 M. Liu, Y. Lu and W. Chen, *Adv. Funct. Mater.*, 2013, **23**, 1289.

26 Y. Lu, Y. Jiang and W. Chen, *Nano Energy*, 2013, **2**, 836.

27 S.-W. Bain, Z. Ma, Z.-M. Cui, L.-S. Zhang, F. Niu and W.-G. Song, *J. Phys. Chem. C*, 2008, **112**, 11340.

28 H. Jia, X. Bai and L. Zheng, *CrystEngComm*, 2012, **14**, 2920.

29 L. Guo, J. Bai, C. Li, Q. Meng, H. Liang, W. Sun, H. Li and H. Liu, *Appl. Surf. Sci.*, 2013, **283**, 107.

30 J. Xiao and L. Qi, *Nanoscale*, 2011, **3**, 1383.

31 X. Huang, E. Zhu, Y. Chen, Y. Li, C.-Y. Chiu, Y. Xu, Z. Lin, X. Duan and Y. Huang, *Adv. Mater.*, 2013, **25**, 2974.

32 H. Zhang, B. Chen and J. F. Banfield, *J. Phys. Chem. C*, 2010, **114**, 14876.

33 C. J. DeSantis, A. A. Peverly, D. G. Peters and S. E. Skrabalak, *Nano Lett.*, 2011, **11**, 2164.

34 L. Wang, Y. Nemoto and Y. Yamauchi, *J. Am. Chem. Soc.*, 2011, **133**, 9674.

35 B. Lim and Y. Xia, *Angew. Chem. Int. Ed.*, 2011, **50**, 76.

36 L. Wang and Y. Yamauchi, *Chem. Mater.*, 2009, **21**, 3562.

37 C. Hu, Y. Guo, J. Wang, L. Yang, Z. Yang, Z. Bai, J. Zhang, K. Wang and K. Jiang, *ACS Appl. Mat. Interfaces*, 2012, **4**, 4461.

38 C. Xu, L. Cheng, P. Shen and Y. Liu, *Electrochem. Commun.*, 2007, **9**, 997.

39 K. Ding, Y. Wang, H. Yang, C. Zheng, YanliCao, H. Wei, Y. Wang and Z. Guo, *Electrochim. Acta*, 2013, **100**, 147.

40 Y. Yamauchi, A. Tonegawa, M. Komatsu, H. Wang, L. Wang, Y. Nemoto, N. Suzuki and K. Kuroda, *J. Am. Chem. Soc.*, 2012, **134**, 5100.

41 S. Du, *Int. J. Low-Carbon Technol.*, 2012, **7**, 44.

42 H. Lee, S. E. Habas, G. A. Somorjai and P. Yang, *J. Am. Chem. Soc.*, 2008, **130**, 5406.

43 B. Y. Xia, H. B. Wu, X. Wang and X. W. Lou, *J. Am. Chem. Soc.*, 2012, **134**, 13934.

44 C. Zhu, S. Guo and S. Dong, *Chem.Eur. J.*, 2013, **19**, 1104.

45 Y.-N. Wu, S.-J. Liao, Z.-X. Liang, L.-J. Yang and R.-F. Wang, *J. Power Sources*, 2009, **194**, 805.

46 C. Li and Y. Yamauchi, *Phys. Chem. Chem. Phys.*, 2013, **15**, 3490.

47 H. Wang, L. Wang, T. Sato, Y. Sakamoto, S. Tominaka, K. Miyasaka, N. Miyamoto, Y. Nemoto, O. Terasaki and Y. Yamauchi, *Chem. Mater.*, 2012, **24**, 1591.

48 C. Hu, H. Cheng, Y. Zhao, Y. Hu, Y. Liu, L. Dai and L. Qu, *Adv. Mater.*, 2012, **24**, 5493.

49 X. Niu, H. Zhao, C. Chen and M. Lan, *Chem. Cat. Chem.*, 2013, **5**, 1416.

50 N. V. Long, T. Duy Hien, T. Asaka, M. Ohtaki and M. Nogami, *Int. J. Hydrogen Energy*, 2011, **36**, 8478.

51 B. Y. Xia, W. T. Ng, H. B. Wu, X. Wang and X. W. Lou, *Angew. Chem.*, 2012, **124**, 7325.

Captions

Fig. 1 Low (A), medium (B), and high magnification (C, D, E, F) TEM images of the Pt-Pd NDs. Insets show the particle size distribution (in Fig. 1A) and the SAED pattern of the Pt-Pd NDs (in Fig. 1B).

Fig. 2 HAADF-STEM-EDS mapping images (A-C) and line scanning profiles of the Pt-Pd nanodendrite (D).

Fig. 3 XRD (A), EDS (B), and high resolution Pt 4f (C) and Pd 3d (D) XPS spectra of the Pt-Pd NDs.

Fig. 4 TEM images of the products synthesized at different Pt/Pd molar ratios: 0:1 (A), 1:0 (B), 2:1 (C), and 1:2 (D).

Fig. 5 Schematic illustration of the formation mechanism of the Pt-Pd NDs.

Fig. 6 TEM images of the Pt-Pd products prepared with different reaction time: 1 min (A), 5 min (B), 30 min (C), and 2 h (D).

Fig. 7 CO-stripping voltammograms of the Pt-Pd NDs (A), Pt-black (B), and Pd-black (C) catalysts modified electrodes in 0.5 M H_2SO_4 at a scan rate of 50 mV s^{-1}.

Fig. 8 Cyclic voltammograms of the Pt-Pd NDs (curve a), Pt-black (curve b), and Pd-black (curve c) catalysts modified electrodes in 1.0 M KOH containing 1.0 M methanol (A) and 1.0 M EG (B), respectively.

Fig. 9 Chronoamperometric curves of the Pt-Pd NDs (curve a), Pt-black (curve b), and Pd-black (curve c) catalysts modified electrodes in 1.0 M KOH containing 1.0 M methanol (A) and 1.0 M EG (B) by applying an potential of −0.2 V, respectively. The plots of the forward peak current densities (*j*) on the Pt-Pd NDs modified electrodes with the number cycles in 1.0 M KOH containing 1.0 M methanol (C) and 1.0 M EG (D), respectively. Insets (Fig. 9C and D) are the corresponding 1st, 250th, and 500th cyclic voltammograms at a scan rate of 50 mV s^{-1}.

Figures

Fig. 1

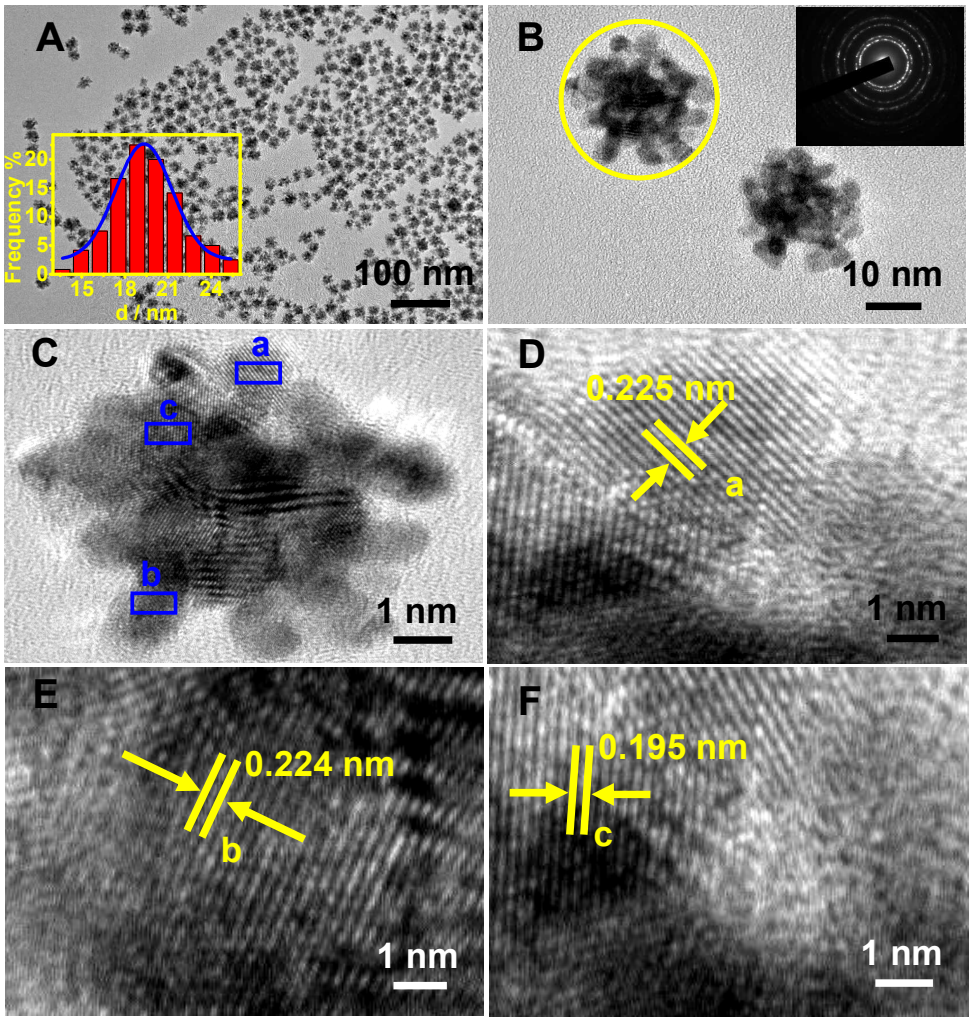

Fig. 2

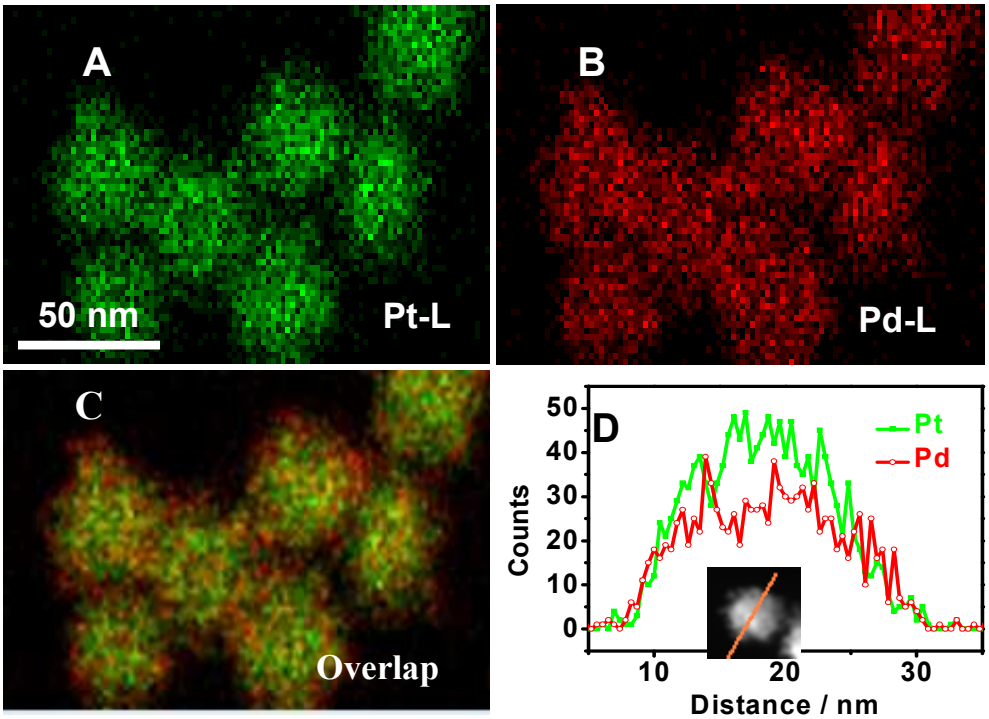

Fig. 3

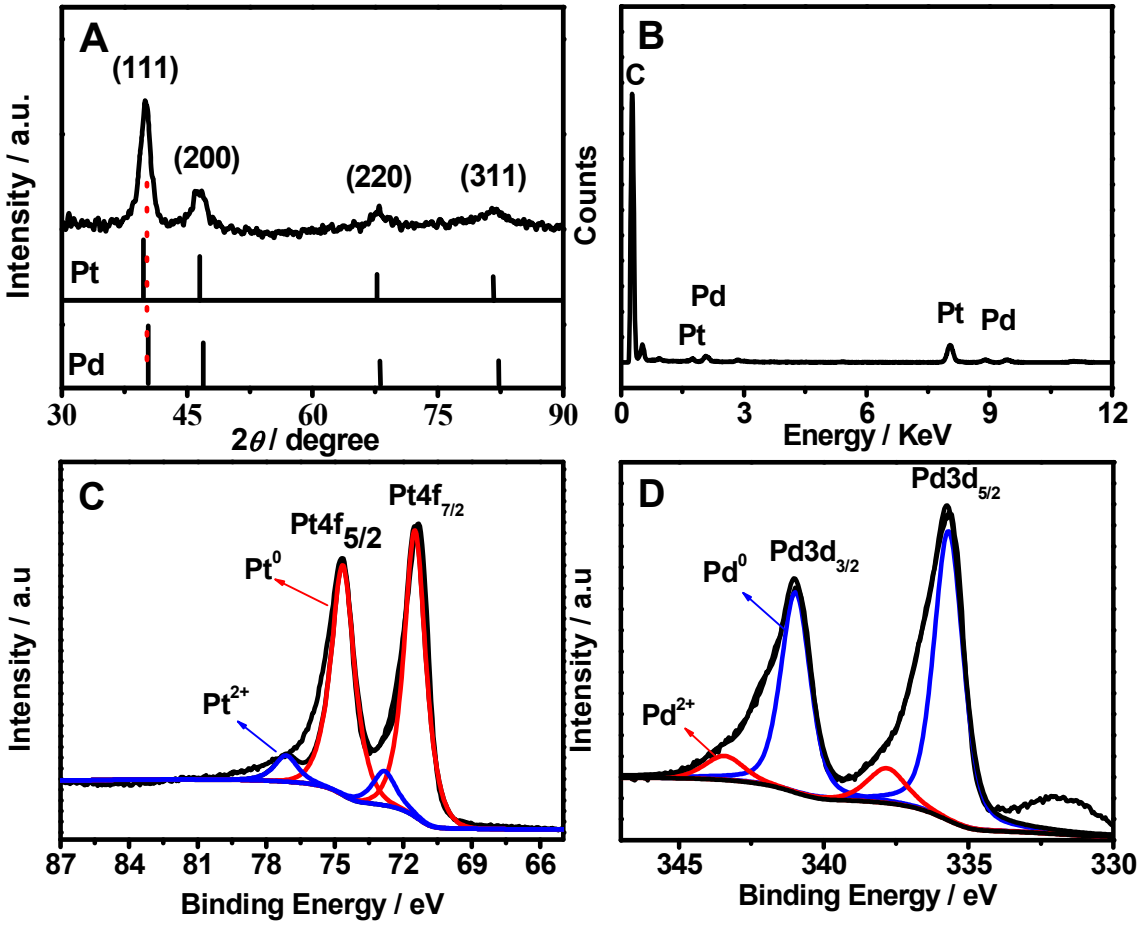

Fig. 4

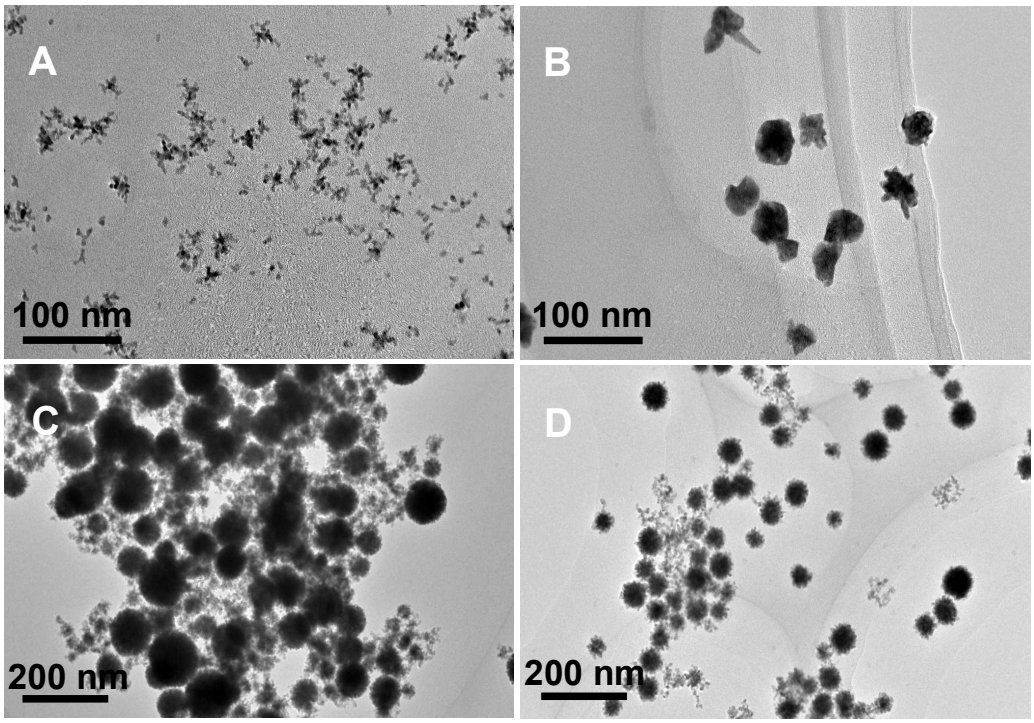

Fig. 5

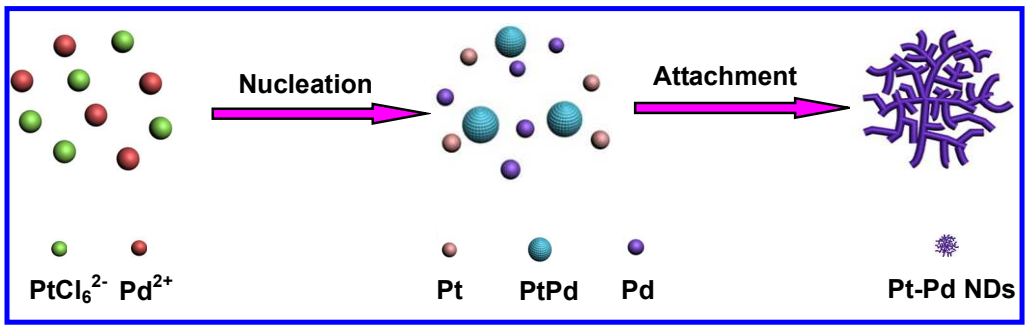

Fig. 6

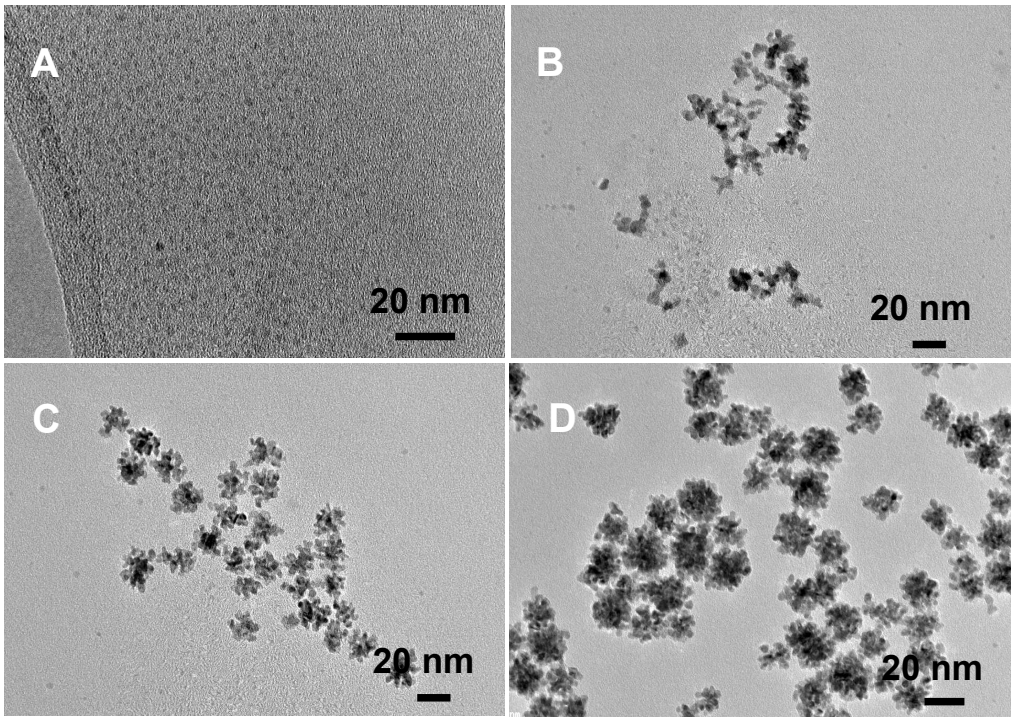

Fig. 7

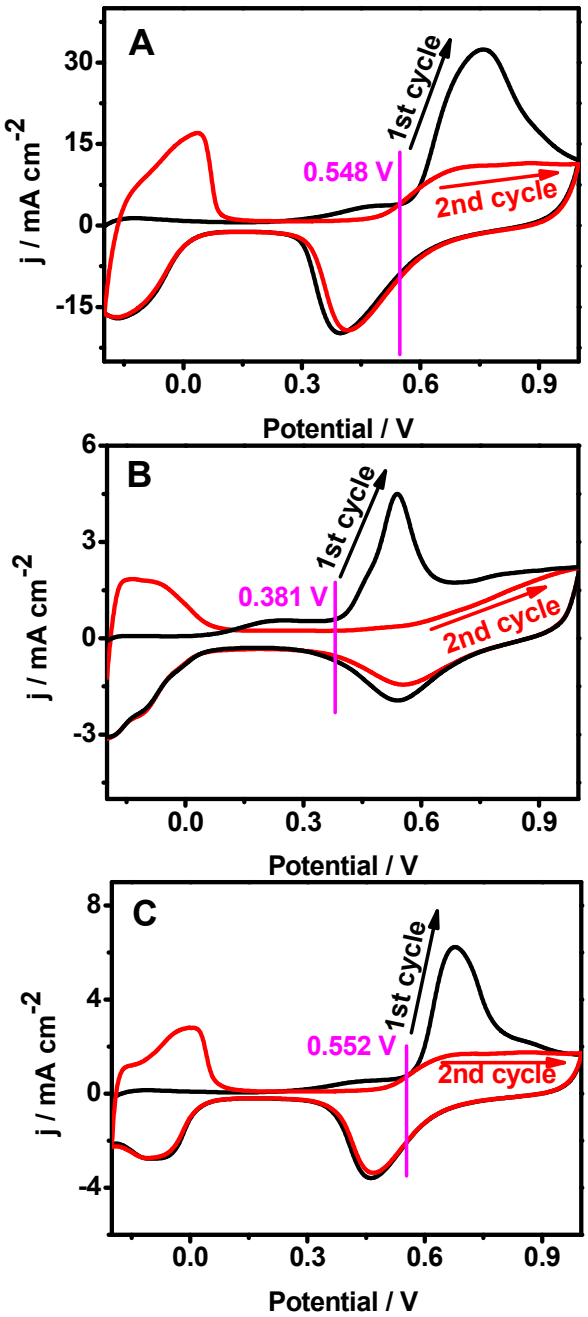

Fig. 8

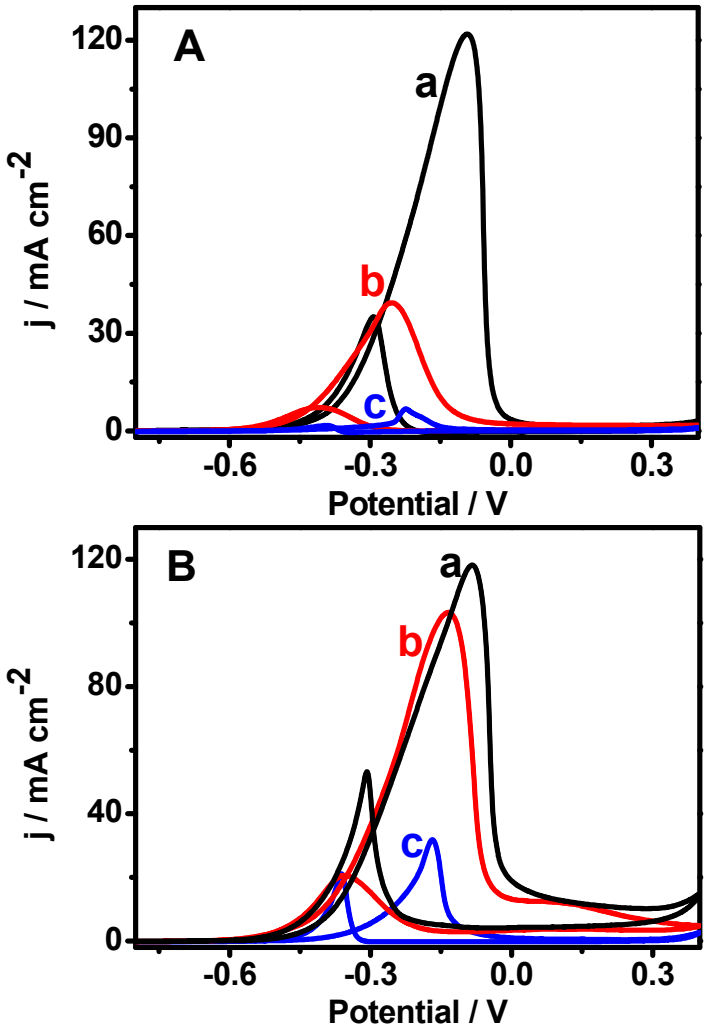

Fig. 9